

# On the Stimulation Artifact Reduction during Electrophysiological Recording of Compound Nerve Action Potentials\*

Raphael Panskus<sup>1,2</sup>, Lukas Holzapfel<sup>2</sup>, Wouter A. Serdijn<sup>1,3</sup>, *Fellow, IEEE*, and Vasiliki Giagka<sup>1,2</sup> *Senior Member, IEEE*

**Abstract**—Recording neuronal activity triggered by electrical impulses is a powerful tool in neuroscience research and neural engineering. It is often applied in acute electrophysiological experimental settings to record compound nerve action potentials. However, the elicited neural response is often distorted by electrical stimulus artifacts, complicating subsequent analysis. In this work, we present a model to better understand the effect of the selected amplifier configuration and the location of the ground electrode in a practical electrophysiological nerve setup. Simulation results show that the stimulus artifact can be reduced by more than an order of magnitude if the placement of the ground electrode, its impedance, and the amplifier configuration are optimized. We experimentally demonstrate the effects in three different settings, in-vivo and in-vitro.

## I. INTRODUCTION

Electrically evoked compound action potentials (eCAPs) propagating along a peripheral nerve are commonly studied to elucidate neuronal functions or evaluate the safety and efficacy of neural therapies [1], [2]. Depending on the diameter and myelination, eCAPs can propagate at 1 m/s to 100 m/s with a duration of approximately 1 ms [3] with an amplitude of the order of a few  $\mu\text{V}$  to 2 mV [4]. However, the recorded signals are often contaminated by stimulus-related artifacts [2]. The stimulus artifact (SA) may appear as a sharp, transient waveform in the recording that usually lasts a few milliseconds and whose amplitude is much larger than the underlying neural activity. Often, these artifacts can obscure the neural signals or saturate the recording amplifier, resulting in distortion or signal loss [5]. As a result, several different artifact reduction techniques have been proposed [6]–[24]. These methods can be categorized into hardware-based [6], [7], software-based [8]–[20], and experimental design-based [21]–[24]. However, hardware engineering techniques for artifact reduction are usually application specific, expensive, and time-consuming to develop. Furthermore, most of these techniques are limited to short artifact durations that do not overlap with the neural response and suffer from an inability to adapt to the dynamic change of SA. It should be noted that software-based methods can

\*Research supported by the Moore4Medical project funded by the ECSEL Joint Undertaking under grant number H2020-ECSEL-2019-IA-876190, and the Fraunhofer Attract fellowship programme

<sup>1</sup>Dept. of Microelectronics, Faculty of Electrical Engineering, Mathematics and Computer Science, Delft University of Technology, The Netherlands.

<sup>2</sup>Dept. of System Integration and Interconnection Technologies, Fraunhofer Institute for Reliability and Microintegration IZM, Berlin, Germany.

<sup>3</sup>Neuroscience Dept., Erasmus Medical Center, Rotterdam, the Netherlands.

Corresponding author e-mail: r.panskus@tudelft.nl

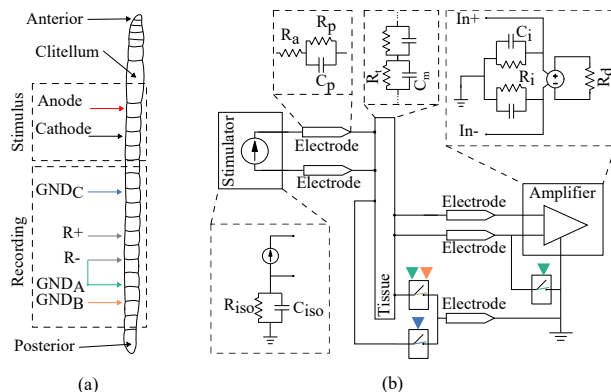


Fig. 1. Schematic representation of a typical experimental setup configuration for the recording of eCAPs. Three different ground electrode placements are indicated by the green, orange and blue arrows for the topologies A, B and C respectively. (a) Electrode placement on an earthworm is shown. R- and R+ = inputs for the amplifier; GND = ground electrode. (b) Electrical equivalent circuits are shown. Arrows represent closed switches.

only be used if the SA does not lead to saturation of the amplifier. The hardware and software methods are tailored to miniaturized systems [25] but are not always suitable for acute electrophysiological experiments using peripheral nerves. Next to these, experimental design-based techniques have been investigated. [21]–[24], [26]. Proposed rules include low contact impedance, using a large surface area ground electrode, increasing the distance between stimulating and recording sides, using alternating polarity stimulus pairs, placing recording electrodes on equipotential lines, and using differential, instead of single-ended, amplifiers. Although these studies are based on surface electrode recordings, many of their techniques can be transferred to peripheral nerve experiments.

This work aims to improve the understanding of the experimental practice of eCAP recording and the effect of some easy-to-implement methodological guidelines on the SA. To this end, ground electrode placement and impedance, together with amplifier configuration and input impedance, are considered. These are implemented in an electrical equivalent model, and their effect on SA reduction is investigated experimentally and via simulations. The model was developed to mimic an experimental setup for measuring explanted peripheral nerves or similar setups with longitudinally arranged electrodes (Fig. 1).

## II. METHOD

### A. Experimental configuration

The conceptual system overview on which the derived model and the experiments are based is shown in Fig. 1. A constant current stimulator (DS8R, Digitimer Ltd., Hertfordshire, UK) is triggered by a signal generator (33622A, Keysight Technologies Co., Ltd., U.S.A.) to inject periodic pulses into the tissue. The resulting SA and neural signals were acquired using an Intan headstage (RHD2132) and interface board (RHD2000 USB interface board, Intan Technologies, Los Angeles, U.S.A.). Stainless steel pins were used as electrodes. The electrodes had a lead body diameter of 0.33 mm, 15 mm length with a 10 cm cable soldered to it. The experiments were conducted inside a Faraday cage to reduce electrical interference. Electrical pulsed stimuli were delivered as cathodic, monophasic rectangular pulses of 3 mA amplitude, 500  $\mu$ s at a rate of 0.25 Hz. The Intan headstage and controller were used at a sample rate of 20 Ks/s for 1 min recordings.

The experimental arrangement was adapted to account for three different configurations (see Fig. 1) by varying the placement of the ground electrode. Topology A is a single-ended configuration where the ground electrode and the negative input of the amplifier are shorted. This is implemented at the headstage by a default onboard 0- $\Omega$  resistor. The resistor was removed to separate ground and reference electrodes for the differential topologies B and C. In B the ground electrode was placed distally on the recording side, while in C it was connected between the stimulating and the recording sites.

*In-Vitro*: The needle electrodes were placed beneath a saline-soaked cotton piece and used as stimulation and

recording electrodes. The stimulating electrode was placed 2-3 cm away from the recording electrodes.

*In-Vivo*: We also tested the feasibility of the ground electrode configuration in-vivo on earthworms to mimic the nerve tissue. The worms were initially anaesthetized with 10% solution ethanol. Then, the worms were washed in tap water and placed on a Styrofoam base. Electrodes were placed 0.5 cm posterior to the clitellum for stimulation. The recording electrodes were inserted at the posterior end, resulting in a distance of 7 cm from the stimulating electrodes.

### B. Model

The peripheral nerve setup and respective topologies of Fig. 1 were modelled using simplified lumped models in LTspice. Each electrode is defined by a first-order electrical model, commonly referred to as a Randles circuit.  $R_a$  stands for the bulk material of the electrode (access resistance),  $R_p$  for the polarization resistance and  $C_p$  for the polarization capacitance, whereas we refer to  $R_c, R_g$  and  $C_g$  when considering the grounded electrode elements. The initial values ( $R_a = R_c = 50 \Omega$ ,  $R_p = R_g = 10 \Omega$ ,  $C_p, C_g = 30 \text{ nF}$ ) were estimated from electrochemical impedance spectroscopy measurements using the electrodes used in the in-vivo and in-vitro experiments. The recording amplifier is modelled as a voltage-controlled voltage source in order to consider it as ideal as possible and independent of separate amplifier configurations. However, the input impedance is considered to account for typical given electrical characteristics of amplifiers. Input impedance is simulated as parallel impedance. To reflect differential inputs or unipolar inputs with a common reference configuration, the capacitive and resistive elements of each input impedance are matched (referred to as symmetrical input impedance) or mismatched

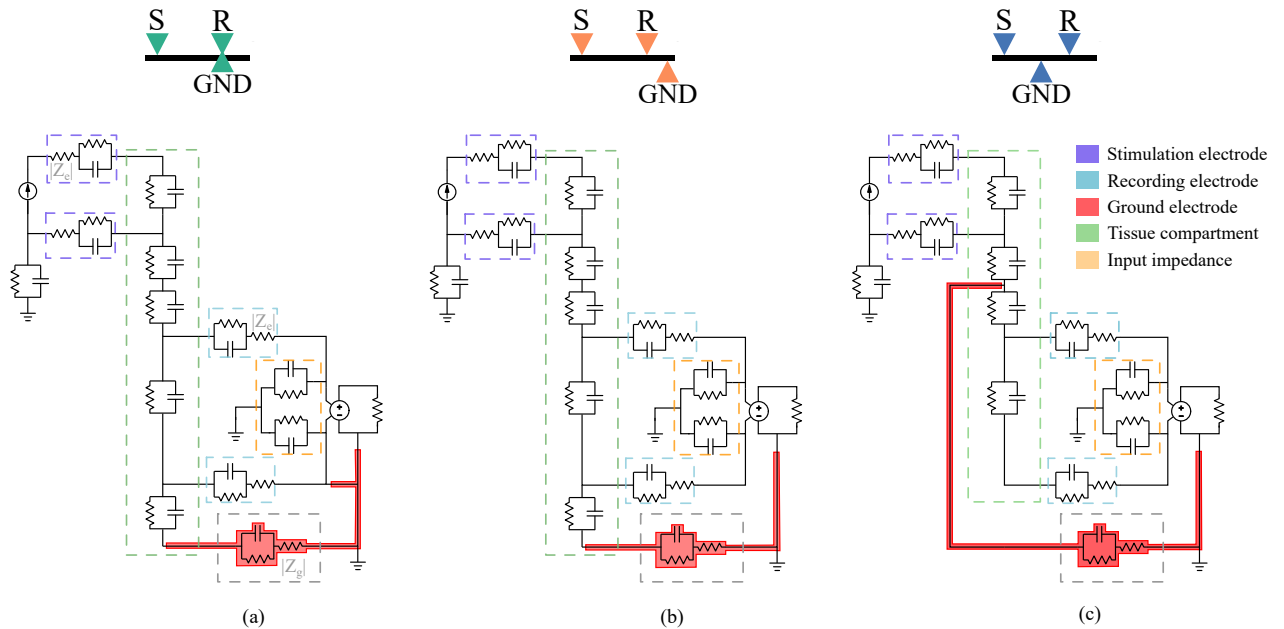


Fig. 2. Topologies of the electrical equivalent circuit models. (a) Schematic of Topology A: Single-ended configuration with shorted ground electrode. (b) Schematic of topology B: Differential configuration and ground electrode placed distal to recording and stimulation side. (c) Schematic of topology C: Differential configuration with the ground electrode placed between stimulation- and recording sides. Illustrations on top of the figure represent each topology with the respective position of electrodes (S = stimulation electrode, R = recording electrodes, GND = ground electrode).

(referred to as non-symmetrical input impedance). Initial values were derived from the data sheets of experimental components with mismatched input impedances ( $R_i = 13 \text{ M}\Omega$ ,  $C_i = 12 \text{ pF}$  for the positive input and  $R_i = 0.5 \text{ M}\Omega$ ,  $C_i = 325 \text{ pF}$  for the negative input). The current stimulator is modelled as a current source with isolation impedance. The isolation aspects are taken into account to match non-ideal conditions. Stimulators are essentially completely isolated from ground but still have some capacitive coupling to it, usually in the order of a few pF. Theoretical values from an isolator unit for the RC circuit were chosen as  $R_{iso} = 10 \text{ T}\Omega$  and  $C_{iso} = 33 \text{ pf}$ , respectively [27]. The contacts between each electrode were electrically interconnected by tissue compartment representations based on a simplified Fricke-Morse model [28], where the intracellular resistance is ignored, reducing the model to the simple  $R_t C_m$  parallel equivalent circuit shown in Fig. 2 ( $R_t$ : extracellular resistance,  $C_m$ : membrane capacitance). Initial values were chosen as  $R_t = 500 \Omega$  and  $C_m = 0.3 \mu\text{F}$ . The circuit model was used to solve for the stimulus artifact injected and measured across the amplifier inputs, resulting from monophasic cathodic stimulation pulses of  $3 \text{ mA}$  amplitude and  $300 \mu\text{s}$ . For each topology, the input impedances were varied from a mismatched input impedance to a matched input impedance. The influence of the ground electrode impedance was also investigated by changing the initial values of  $R_c, R_g$  and  $C_g$ , resulting in an effective impedance  $|Z_g|$  decrease and increase by a factor of 10. ( $|Z_{g1}|$ :  $R_g = 1 \text{ k}\Omega$ ,  $R_c = 5 \Omega$ ,  $C_g = 300 \text{ nF}$ ,  $|Z_{g2}|$ :  $R_g = 10 \text{ k}\Omega$ ,  $R_c = 50 \Omega$ ,  $C_g = 30 \text{ nF}$ ,  $|Z_{g3}|$ :  $R_g = 100 \text{ k}\Omega$ ,  $R_c = 500 \Omega$ ,  $C_g = 3 \text{ nF}$ ). Fig. 2 gives an overview of the complete models for each topology, each of which consists of the current stimulator, two stimulation electrodes, tissue compartments, the recording amplifier with two recording electrodes and a ground electrode.

### C. Offline Signal Processing and Data Analysis

The artifact signals of each measurement, acquired by the Intan system, were separated into subtrials by 25 ms windows using the trigger signals provided by the stimulator. A 2nd-order Butterworth notch filter with a centre frequency of 50 Hz was applied to the data to reduce the main noise. We quantified the recorded artifact by the peak-to-peak amplitude of each setting. In addition, baseline correction was used 5 ms after stimulus onset to avoid unwanted drifts in the extracted windows. Stimulus-triggered averaging of the trials was applied. Based on the conduction velocities of earthworms the first evoked response after stimulus onset is defined as median giant fibre (MGF) and the second response as lateral giant fibre (LGR) activity. All the signal processing and data analysis were performed using Python.

## III. RESULTS AND DISCUSSION

### A. Simulations

*Influence of ground electrode placement:* Fig. 3 shows simulation results for the different ground electrode configurations. In all topologies, current flowing into the tissue compartment in front of the amplifier creates a voltage drop

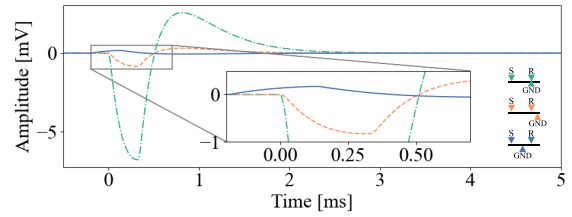


Fig. 3. Simulated SA at the amplifier input for topology A (green), B (orange), C (blue) and initial values of  $|Z_g|$  are shown.

over the compartment, which is added to the recording, i.e., a stimulus artifact. The SA has the greatest amplitude for topology A, resulting from referencing the input signal to ground. Therefore, only the input signal of the positive channel is amplified and not the actual difference of the two input electrodes. Separating the reference electrode from the ground reduces the artifact by changing the configuration from a single-ended to a differential input (topology B and C). The remaining artifact results from the unequal current flowing into the electrodes. This is caused by the non-ideal amplifier and its imbalanced input impedance. The artifact can be further reduced by placing the ground electrode between the stimulation and recording side, as depicted in topology C. In this scenario, creating a direct path to the ground reduces the current in the tissue compartments in front of the amplifier inputs.

*Influence of amplifier input impedance:* In Fig. 4, the peak-to-peak amplitudes for all three topologies with symmetrical and non-symmetrical input impedances, only considering the initial values for  $|Z_g|$  are shown on a logarithmic scale. The symmetrical input impedance configuration in Topology A has no effect on the reduction of SA amplitude. This is because the negative input of the amplifier is shorted to ground. Thus, topology A effectively represents an unbalanced input impedance in both configurations. The voltage at the positive input of the amplifier is mainly determined by the input impedance and electrode-tissue interface. However, the symmetrical input impedance has an influence on topologies B and C and leads to a significant reduction in SA amplitude. The symmetrical input impedance for topology C still results in a residual SA due to the non-ideal amplifier and the resulting voltage across the tissue compartment between the recording electrodes.

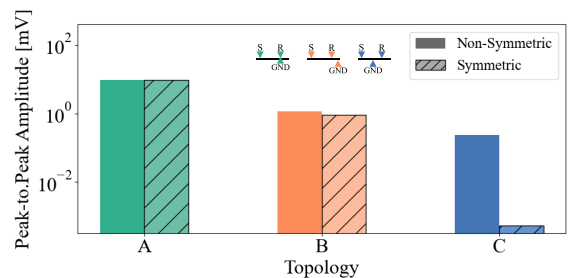


Fig. 4. Simulation results comparing peak-to-peak SA voltages at the amplifier input for topology A (green), B (orange), C (blue). Symmetrical (striped) and non-symmetrical (solid) amplifier input impedance for initial values of  $|Z_g|$  are shown.

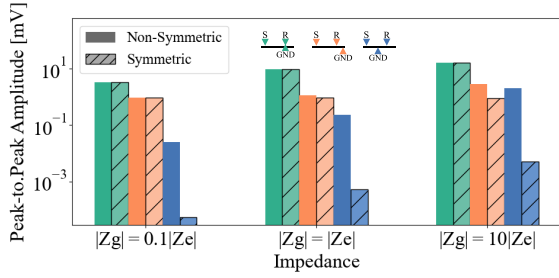


Fig. 5. Simulation results comparing peak-to-peak SA voltages at the amplifier input for topology A (green), B (orange), C (blue). Symmetrical (striped) and non-symmetrical (solid) amplifier input impedance for different values of  $|Z_g|$  are shown.

*Influence of ground electrode impedance:* Fig. 5 shows the peak-to-peak amplitudes for all three topologies and different ground impedances on a logarithmic scale. For all non-symmetrical configurations, the SA increases with increased ground electrode impedance. While an increase of the SA with an increased ground impedance for the symmetrical topology A and C can be recognized, the SA decreases for topology B with symmetrical input impedances. This can be explained by the fact the impedance of the ground electrode shifts the ratio of the voltage divider between the amplifier inputs and the ground electrode. However, no SA change can be observed between the symmetrical and non-symmetrical input impedance of topology A. This is attributable to the same effect that has already been described. For configuration C, clearly, a good tissue-electrode connection and impedance of the ground electrode is needed. Otherwise, the current in the tissue path is increased. It should be noted that low electrode contact impedances on the recording side have no effect on the stimulus artifact when the amplifier input impedance is substantially larger than the electrode impedance. However, the electrode impedance can affect the signal-to-noise ratio (SNR) level. A reduced ground electrode impedance will help decrease the noise in the ground path and increase the SNR for all three configurations.

### B. Experiments

*In-Vitro:* Fig. 6 illustrates recorded SA during the in vitro experiments. Compared to the single-ended topology, the differential amplifier reduced the magnitude of the stimulus artifact by 53% for topology B and by 88% for topology C. Conversely, the configuration of the single-ended amplifier saturated the amplifier with the same stimulus amplitude. Even with the use of the separated ground electrode (topology B), there remained a relatively large amplitude compared to the configuration where the ground electrode is placed between the stimulus and recording side. Based on the electrode configuration, a decreased SNR could be observed. The decreased SNR can also be attributed to the electrode placement. Thus, interfering signals coupling to the stimulation side are diverted by the ground electrode in the middle, while both differential configurations suppress couplings in the ground electrode.

*In-Vivo:* Recordings of in vivo signals are shown in Fig. 7. Again, the effect of electrode placement for topologies B and

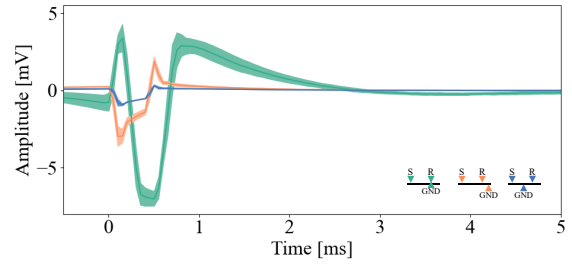


Fig. 6. Average and standard deviation of recorded SA in-vitro for topology A (green), B (orange), C (blue).

C can be observed in the experiments. We have been able to subtract eCAPs from the differential recording while the amplifier saturates in the single-ended topology (results not shown). The eCAP waveforms recorded in the two configurations were of similar magnitude and were qualitatively similar, with an extracellular recording of the median giant fibre (MGF) followed by a later, larger in amplitude lateral giant fibre (LGF) response. The peak-to-peak magnitudes were on the order of  $30\mu\text{V}$  for MGF and  $60\mu\text{V}$  for LGF responses and eCAP latencies in the range of 7 ms to 13 ms.

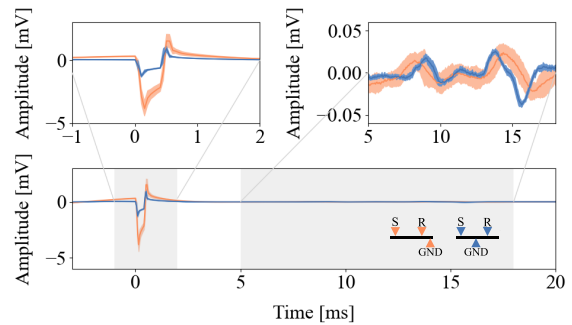


Fig. 7. Averaged SA and eCAPs with standard deviation in-vivo for topology B (orange), C (blue). The top figures show a magnified view of the SA (left) and eCAPs (right), consisting of MGF and LGF responses.

## IV. CONCLUSION

This work demonstrates the possibility of reducing the stimulus artifact when using simple guidelines in acute electrophysiological eCAP experiments. We presented a model to estimate the stimulation artifact from electrical stimulation and evaluated the model in in-vitro and in-vivo experiments. The model considers the influence of the ground electrode placement, amplifier configuration and ground electrode impedance on the stimulus artifact. We have found a differential amplifier configuration with balanced input impedances and a ground electrode with low electrode-tissue impedance between the stimulation and recording sides to be an effective topology for reducing stimulation artifacts. The learnings from this study will be integrated into future electrophysiological eCAP experiments.

## ACKNOWLEDGMENT

The authors would like to thank P. A. Dardagan for assisting with data collection and processing; K. Kolovou-Kouri and J. Wilson, for their critical review of the manuscript.

## REFERENCES

- [1] M. V. Accardi, M. K. Pugsley, R. Forster, E. Troncy, H. Huang, and S. Authier, "The emerging role of in vitro electrophysiological methods in CNS safety pharmacology," *Journal of Pharmacological and Toxicological Methods*, vol. 81, pp. 47–59, 2016. DOI: 10.1016/J.VASCN.2016.03.008.
- [2] J. L. Parker, N. H. Shariati, and D. M. Karantonis, "Electrically evoked compound action potential recording in peripheral nerves," *Bioelectronics in Medicine*, vol. 1, no. 1, pp. 71–83, 2017. DOI: 10.2217/BEM-2017-0005.
- [3] M. B. Bromberg, "An electrodiagnostic approach to the evaluation of peripheral neuropathies," *Physical Medicine and Rehabilitation Clinics*, vol. 24, no. 1, pp. 153–168, 2013. DOI: 10.1016/j.pmr.2012.08.020.
- [4] S. He, H. F. Teagle, and C. A. Buchman, "The electrically evoked compound action potential: From laboratory to clinic," *Frontiers in Neuroscience*, vol. 11, no. JUN, p. 339, 2017. DOI: 10.3389/fnins.2017.00339.
- [5] Y. Liu, A. Urso, R. Martins Da Ponte, et al., "Bidirectional Bioelectronic Interfaces: System Design and Circuit Implications," *IEEE Solid-State Circuits Magazine*, vol. 12, no. 2, pp. 30–46, 2020. DOI: 10.1109/MSSC.2020.2987506.
- [6] A. de Cheveigné and I. Nelken, "Filters: when, why, and how (not) to use them," *Neuron*, vol. 102, no. 2, pp. 280–293, 2019. DOI: 10.1016/j.neuron.2019.02.039.
- [7] X. Liu, J. Li, T. Chen, W. Wang, and M. Je, "A Neural Recording and Stimulation Chip with Artifact Suppression for Biomedical Devices," *Journal of Healthcare Engineering*, vol. 2021, 2021. DOI: 10.1155/2021/4153155.
- [8] D. J. Caldwell, J. A. Cronin, R. P. N. Rao, et al., "Signal recovery from stimulation artifacts in intracranial recordings with dictionary learning," *Journal of neural engineering*, vol. 17, no. 2, p. 26023, 2020. DOI: 10.1088/1741-2552/ab7a4f.
- [9] D. A. Wagenaar and S. M. Potter, "Real-time multi-channel stimulus artifact suppression by local curve fitting," *Journal of neuroscience methods*, vol. 120, no. 2, pp. 113–120, 2002. DOI: 10.1016/S0165-0270(02)00149-8.
- [10] L. F. Heffer and J. B. Fallon, "A novel stimulus artifact removal technique for high-rate electrical stimulation," *Journal of neuroscience methods*, vol. 170, no. 2, pp. 277–284, 2008. DOI: 10.1016/j.jneumeth.2008.01.023.
- [11] M. B. Voigt, P. A. Yusuf, and A. Kral, "Intracortical microstimulation modulates cortical induced responses," *Journal of Neuroscience*, vol. 38, no. 36, pp. 7774–7786, 2018. DOI: 10.1523/JNEUROSCI.0928-18.2018.
- [12] D. J. O'Shea and K. V. Shenoy, "ERAASR: an algorithm for removing electrical stimulation artifacts from multielectrode array recordings," *Journal of neural engineering*, vol. 15, no. 2, p. 26020, 2018. DOI: 10.1088/1741-2552/aaa365.
- [13] R. Brash, W. Serdijn, and D. G. Muratore, "FARA: A Fast Artifact Recovery Algorithm with Optimum Stimulation Waveform for Single-Cell Resolution Massively Parallel Neural Interfaces," in *2022 IEEE International Symposium on Circuits and Systems (ISCAS)*, IEEE, 2022, pp. 190–194. DOI: 10.1109/ISCAS48785.2022.9937814.
- [14] K. Kolodziej, M. Szypulska, W. Dabrowski, and P. Hottowy, "Modelling and Cancellation of the Stimulation Artifact for ASIC-based Bidirectional Neural Interface," *Proceedings of 25th International Conference Mixed Design of Integrated Circuits and Systems, MIXDES 2018*, pp. 449–453, 2018. DOI: 10.23919/MIXDES.2018.8436947.
- [15] P. Hottowy, A. Skoczeń, D. E. Gunning, et al., "Properties and application of a multichannel integrated circuit for low-artifact, patterned electrical stimulation of neural tissue," *Journal of Neural Engineering*, vol. 9, no. 6, p. 066005, 2012. DOI: 10.1088/1741-2560/9/6/066005.
- [16] T. Hashimoto, C. M. Elder, and J. L. Vitek, "A template subtraction method for stimulus artifact removal in high-frequency deep brain stimulation," *Journal of neuroscience methods*, vol. 113, no. 2, pp. 181–186, 2002. DOI: 10.1016/S0165-0270(01)00491-5.
- [17] E. B. Montgomery Jr, J. T. Gale, and H. Huang, "Methods for isolating extracellular action potentials and removing stimulus artifacts from microelectrode recordings of neurons requiring minimal operator intervention," *Journal of neuroscience methods*, vol. 144, no. 1, pp. 107–125, 2005. DOI: 10.1016/j.jneumeth.2004.10.017.
- [18] S. Culaclii, B. Kim, Y.-K. Lo, and W. Liu, "A hybrid hardware and software approach for cancelling stimulus artifacts during same-electrode neural stimulation and recording," in *2016 38th Annual International Conference of the IEEE Engineering in Medicine and Biology Society (EMBC)*, IEEE, 2016, pp. 6190–6193. DOI: 10.1109/EMBC.2016.7592142.
- [19] S. Culaclii, B. Kim, Y. K. Lo, L. Li, and W. Liu, "Online Artifact Cancellation in Same-Electrode Neural Stimulation and Recording Using a Combined Hardware and Software Architecture," *IEEE Transactions on Biomedical Circuits and Systems*, vol. 12, no. 3, pp. 601–613, 2018. DOI: 10.1109/TBCAS.2018.2816464.
- [20] P. C. Klink, B. Dagnino, M.-A. Gariel-Mathis, and P. R. Roelfsema, "Distinct feedforward and feedback effects of microstimulation in visual cortex reveal neural mechanisms of texture segregation," *Neuron*, vol. 95, no. 1, pp. 209–220, 2017. DOI: 10.1016/j.neuron.2017.05.033.
- [21] K. C. McGill, K. L. Cummins, L. J. Dorfman, et al., "On the nature and elimination of stimulus artifact in nerve signals evoked and recorded using surface electrodes," *IEEE Transactions on Biomedical Engineering*, no. 2, pp. 129–137, 1982. DOI: 10.1109/TBME.1982.325019.
- [22] L. McLean, R. N. Scott, and P. A. Parker, "Stimulus artifact reduction in somatosensory evoked potential acquisition: A conceptual model," in *Proceedings of 17th International Conference of the Engineering in Medicine and Biology Society*, IEEE, vol. 2, 1995, pp. 909–910. DOI: 10.1109/IEMBS.1995.579293.
- [23] R. N. Scott, L. McLean, and P. A. Parker, "Stimulus artefact in somatosensory evoked potential measurement," *Medical and Biological Engineering and Computing*, vol. 35, pp. 211–215, 1997. DOI: 10.1007/BF02530040.
- [24] G. Wu, A. Belzberg, J. Nance, S. Gutierrez-Hernandez, E. K. Ritzl, and M. Ringkamp, "Artifact reduction by using alternating polarity stimulus pairs in intraoperative peripheral nerve action potential recording," *Journal of Clinical Monitoring and Computing*, vol. 35, no. 6, pp. 1467–1475, 2021. DOI: 10.1007/s10877-020-00613-9.
- [25] V. Giagka and W. A. Serdijn, "Realizing flexible bioelectronic medicines for accessing the peripheral nerves – technology considerations," *Bioelectronic Medicine 2018 4:1*, vol. 4, no. 1, pp. 1–10, 2018. DOI: 10.1186/s42234-018-0010-Y.
- [26] K. Chakravarthy, H. Bink, and D. Dinsmoor, "Sensing Evoked Compound Action Potentials from the Spinal Cord: Novel Pre-clinical and Clinical Considerations for the Pain Management Researcher and Clinician," *Journal of pain research*, vol. 13, pp. 3269–3279, 2020. DOI: 10.2147/JPR.S289098.
- [27] J. E. Ross, D. F. Lovely, and P. A. Parker, "Design of a PC controlled constant current stimulator for evoked potential studies," *Annual International Conference of the IEEE Engineering in Medicine and Biology - Proceedings*, vol. 4, pp. 2594–2596, 2000. DOI: 10.1109/IEMBS.2000.901388.
- [28] J. L. Damez, S. Clerjon, S. Abouelkaram, and J. Lepetit, "Dielectric behavior of beef meat in the 1–1500 kHz range: Simulation with the Fricke/Cole–Cole model," *Meat Science*, vol. 77, no. 4, pp. 512–519, 2007. DOI: 10.1016/J.MEATSCI.2007.04.028.